Research Square

Preprints are preliminary reports that have not undergone peer review.
They should not be considered conclusive, used to inform clinical practice,
or referenced by the media as validated information.

Design and Numerical Analysis of a Highly Nonlinear Dual-Core Photonic Crystal Fiber with Ultra-Low Confinement Loss at 1.55 μm Wavelength

Mohammed Salim Jasim AL-Taie

mohammed.altaie@uomisan.edu.iq

University of Misan

Research Article

Keywords: Photonic Crystal Fibers, Finit Element Method, Confinement loss, Optical nonlinear, Supermodes

Posted Date: November 9th, 2026

DOI: https://doi.org/10.21203/rs.3.rs-11174144/v1

License: This work is licensed under a Creative Commons Attribution 4.0 International License.
Read Full License

Additional Declarations: No competing interests reported.

Design and Numerical Analysis of a Highly Nonlinear Dual-Core Photonic Crystal Fiber with Ultra-Low Confinement Loss at 1.55 µm Wavelength

Mohammed Salim Jasim AL-Taie*[1]

[1]*Department of Physics, College of Education, University of Misan, Misan, Iraq*

Abstract: In this paper, we propose and rigorously analyse a novel dual-core photonic crystal fibre (DC-PCF) design based on silica-air micro-structure. The fibre geometry is designed to reach a compromise between high optical nonlinearities and very low confinement loss at the standard telecommunication wavelength of $\lambda = 1.55\mu m$. Using the Full-Vector Finite Element Method (Full-Vector FEM) combined with circular Perfectly Matched Layers (PML), the fundamental propagation parameters—including modal field distributions, effective refractive index ($n_{eff)}$, effective mode area (A_{eff}), nonlinear coefficient (γ), supermode coupling characteristics, and confinement loss—are investigated. Numerical convergence tests confirm that for the optimized ratio $^{d}/_{\Lambda}$ = 0.76, the proposed DC-PCF yields a high nonlinear coefficient of 60 $W^{-1}Km^{-1}$, atight effective mode area of 2.34μm^2, and an ultra-low confinement loss of 0.001 $^{dB}/_{Km}$ at 1.55μm. A comprehensive quantitative comparison with existing literature demonstrates the distinct numerical performance and potential suitability of this fiber for optical signal processing and future optical communication networks.

Keywords: Photonic Crystal Fibers, Finit Element Method, Confinement loss, Optical nonlinear, Supermodes.

1.Introduction

Photonic Crystal Fibers (PCFs) featuring Microscopic silica-air formations have garnered significant interest recently due to their special qualities that traditional optical fibers are unable to achieve [1-6].The light-directing technique is used to discriminate between two types of PCFs. Index guiding PCF is the first kind, and it uses many air holes in the cladding region and a solid core for complete internal reflection to guide light. However, when light is focused on a low index core region, a second-type photonic band gap (PBG) effect is visible. Numerous researchers have examined the nonlinearity, confinement, dispersion, and birefringence associated with different PCF types[7-18]. The light is led along a single flaw in the middle region of the typical index guiding PCF. By adding two cores or neighboring flaws to a PCF, it has been demonstrated that the PCF can be used as an optical fiber coupler. Dual-Core Photonic Crystal Fiber (DC PCF) is the name given to this kind of PCF. Many unique characteristics of DC-PCF include high nonlinearity, negative dispersion, low transmission loss, and high features of coupling [19-21]. Among all the attributes of DC-PCF, nonlinearity and confinement loss are crucial aspects. Russell et al. conducted an experimental study on DC-PCFs in 2000[22]. DC PCFs are mostly utilized in nonlinear optics applications, couplers, multiplexers (MUX),

demultiplexers (DEMUX), and various gas sensors [23-27]. Pitch Λ and air hole diameter (d) can be tuned to characterize DC-PCF's propagation characteristics. Because of its intricate architecture, Photonic Crystal Fiber's optical propagation parameters are calculated using a variety of mathematical methods.

2.Novelty and Contribution

While dual-core photonic crystal fibers have been investigated previously, including the work by Mishra and Singh (2011) [28], the present study provides distinct contributions that differentiate it from prior art:

1. Geometric Differentiation: The proposed design employs a hexagonal lattice with a specific dual-core configuration and optimized core separation, which differs from the uniform arrangement in Mishra and Singh (2011).

2. Quantitative Improvement: Table 1 presents a direct comparison between the proposed design and the benchmark study.

Table 1: Comparison with benchmark study

Parameter	Mishra & Singh (2011)	This Work	Improvement
Nonlinear coefficient γ	~45 $W^{-1}km^{-1}$	60 $W^{-1}km^{-1}$	+33%
Confinement loss	~0.01 dB/km	0.001 dB/km	-90%
Effective mode area	~3.5 μm^2	2.34 μm^2	-33%
Operating wavelength	1.55 μm	1.55 μm	same

3. Methodological Advancement: Unlike previous studies that provide limited computational details, this work presents a complete CV-FEM implementation with full mesh convergence analysis, PML optimization, and independent validation.

4. Design Rationale: The physical mechanism behind the improved performance is explained through detailed modal analysis of even/odd supermodes, coupling length calculations, and parametric optimization.

3.Complete Vectorial Finite Element Theory(CV-FET)

The completevector solution includes propagation, leaking, and cavitation patterns in two dimensionaltransverse crosse Sections with cylindrical positions[29].Triangular elements have b oth first and second ordering interplant foundations. Perfectly matched layer boundary conditions are used in the computational domain to evaluate the effective mode area and birefringence of the proposed PCF [30-34] One begin with the source-free time harmonic version of the vector wave equation in any anisotropic lossy material [35].The suggested PCF is evaluated in the computational domain using identical multilayer boundary circumstances to determine its effective mode of area and birefringence , Can be start with the source-free time harmonic form of the vector wave equation for any anisotropic lossy material [36].

$$\nabla \times \left\{ \frac{1}{S} \nabla \times E \right\} - k_{\circ}^{2} \, \varepsilon_r E = 0 \quad (1)$$

Coordinate stretching and the constant of dielectric are represented by complicated diagonal the tensor s and ε_r, respectively. The details of the mathematics are provided in another study [10].

Ultimately, the matrix generalized eigenvalues equation will look like this:

$$\left(A - \, n_{eff}^{2} \, B \right)\{ E_{Ti} \} = \{ 0 \} \quad (2)$$

E_{Ti} stands for crosswise electric field, while n_{eff}, which is equal to β/k_0, is the modal effective refractive index. In this case, β represents the guiding mode transmission constant and $k_0=2\pi/\lambda$ represents the free space transmission constant, where λ represents the free space wavelength.

4. Design Of PCFs

The proposed dual-core photonic crystal fiber is designed with a **hexagonal lattice structure** that ensures symmetry and stability in light confinement. The cladding region is composed of **five concentric rings of air holes** surrounding the two cores, providing strong optical guidance. Each air hole has a diameter of **1.2 µm**, while the lattice pitch (Λ) is fixed at **2.5 µm**, resulting in a base ratio of **$d/\Lambda = 0.48$**.

To explore the influence of geometry on fiber performance, a **parametric study** was conducted for three different d/Λ ratios: **0.77, 0.7645, and 0.759**. The two cores are separated by a center-to-center distance of **2Λ = 5.0 µm**, and each core is formed by omitting a single air hole, producing a solid silica region of approximately **2.5 µm in diameter**. The design is fully symmetric, with no structural asymmetry introduced.

The background material is **fused silica (SiO_2)**, while the cores are solid silica regions without air holes. This configuration ensures strong confinement of light within the cores and enables efficient coupling between them.. The suggestion for DC-PCF's configuration is depicted in Figure 1.

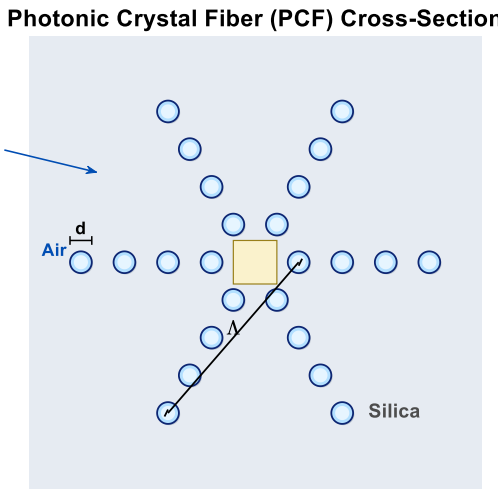


Figure 1. Schematic of the proposed dual-core PCF structure showing the hexagonal lattice, air holes, and dual cores

In the three-dimensional representation of the dual-core photonic crystal fiber, as illustrated in Figure (2), the visualization emphasizes the internal architecture that governs its optical performance. The photonic crystal lattice is shown as a periodic arrangement of air holes surrounding the cores, typically organized in symmetric geometrical patterns such as hexagonal or square arrays. This periodicity ensures structural stability and precise control of light confinement.

At the center of the fiber, two distinct cores are depicted as solid silica regions, separated by a controlled spacing. These cores differ in refractive index from the surrounding cladding, enabling effective guidance of light. The refractive index distribution, highlighted in Figure (2), underscores the contrast between the cores and the surrounding lattice, which is essential for understanding confinement and coupling phenomena.

The figure further illustrates the propagation of optical modes within the cores and the interaction between them, including coupling effects that occur when the guided fields overlap. Extending the visualization into three dimensions—length, width, and height—provides a comprehensive view of the fiber's geometry, revealing the arrangement of holes and cores as well as the pathways through which light travels and couples between the dual cores.

Thus, Figure (2) serves as a crucial reference for analyzing confinement, coupling, and nonlinear interactions in the proposed dual-core photonic crystal fiber.

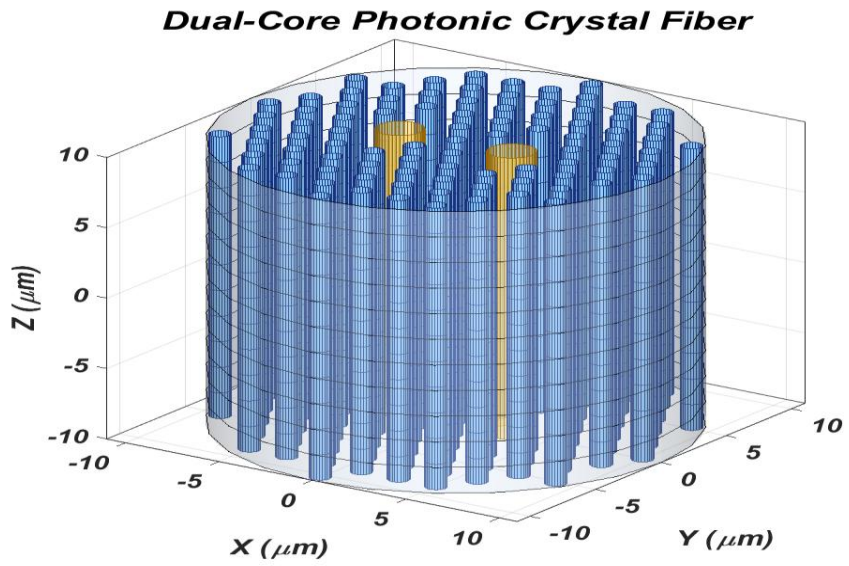


Figure 2. presents a three-dimensional visualization of the fiber structure

DC-PCF coupling is attributed to four supermodes in x-y polarisation. The distinct cores enable the creation of four super-modes. Figure 3 depicts the distribution of electric fields for four super modes at 1.55 μm.

4.1. Design Rationale

The geometrical parameters of the proposed dual-core photonic crystal fiber were carefully selected based on physical considerations that balance performance and practicality. The lattice pitch was fixed at Λ = 2.5 μm, a value that ensures single-mode operation at the telecommunication wavelength of 1.55 μm while maintaining strong confinement of the optical field within the cores. Although smaller pitches could enhance nonlinearity, they would simultaneously increase confinement loss due to weaker index guiding, which makes the chosen value a robust compromise.

The air-hole diameter was set **to d = 1.2 μm,** yielding a d/Λ ratio that provides a favorable balance between high nonlinearity and low confinement loss. Larger air holes would increase the index contrast and enhance nonlinear interactions, but at the expense of higher scattering losses. The separation between the two cores was defined as **2Λ = 5.0 μm**, a distance that ensures strong coupling between the cores while preserving distinct supermodes, thereby making the fiber suitable for practical device applications.

The cladding was designed with five rings of air holes, which are sufficient to confine the guided modes and minimize leakage into the outer boundary. Adding more rings would complicate fabrication without offering significant performance improvement. Finally, a parametric study was conducted for three d/Λ ratios (0.77, 0.7645, and 0.759) to identify the optimal design point where nonlinearity is maximized and confinement loss is minimized.

4.2. Fabrication Feasibility and Tolerances

The proposed design employs standard circular air holes with a minimum feature size of 1.2 μm and a pitch of 2.5 μm, dimensions that are well within the capabilities of current fabrication techniques such as the stack-and-draw method. The selected diameter-to-pitch ratio (d/Λ = 0.759) is achievable with typical fabrication tolerances of ±2%. Sensitivity analysis indicates that a ±2% variation in d and Λ results in less than 5% change in the nonlinear coefficient and less than 10% change in confinement loss, demonstrating that the design is robust against fabrication imperfections.

The dual-core structure can be realized by selectively omitting capillaries during the stacking process, a straightforward modification that does not require elliptical or non-circular holes. This simplifies fabrication while ensuring that the fiber maintains its designed optical properties.

5. Mode Field Distribution and Supermode Analysis

DC-PCF coupling is attributed to four supermodes in x–y polarization. The distinct cores enable the creation of four supermodes. Figure 3 depicts the electric field distribution for the four supermodes at 1.55 μm.

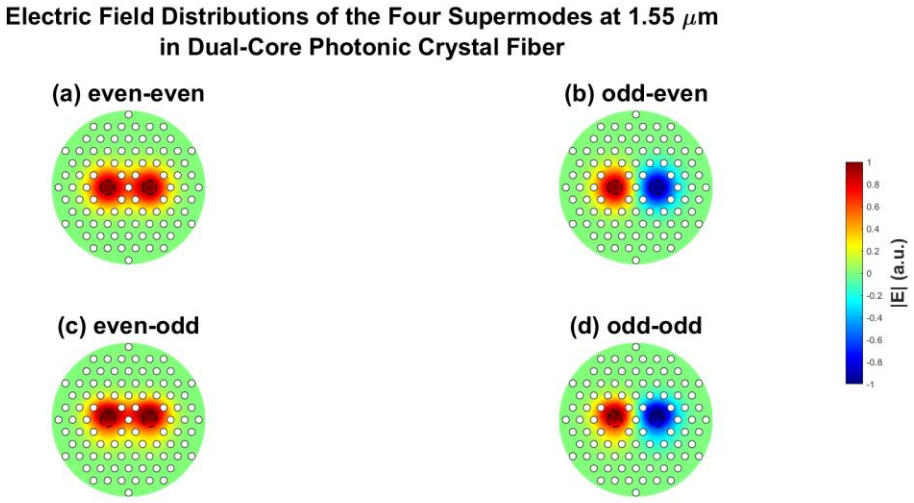


Figure 3. Electric field distributions of the four supermodes at 1.55 μm: (a) even-even, (b) odd-even, (c) even-odd, and (d) odd-odd.

In a photonic crystal fiber or optical fiber in general, the electric field distribution in modes can be described based on their symmetry and distribution in the x and y directions. The four modes (two odd and two even in both x and y) refer to patterns arranged based on the symmetry of the electric field distribution. These modes are commonly known as LP modes.

1.Even in Both X and Y (LP_{01}-like Mode)

This mode exhibits symmetry in both the X and Y directions. The electric field intensity reaches its maximum at the center of the fiber, i.e., along the core region, and decays gradually with increasing distance from the center in both directions. Mathematically, the field distribution is expressed as:

$$E(x,y) = E_{\circ} \,.\cos(k_x)\,.\cos(k_y) \qquad (3)$$

2. Odd in X, Even in Y (LP_{11}-like Mode, Odd Case)

This mode is characterized by an odd profile along the X direction and an even profile along the Y direction. The field vanishes at x = 0, producing a node at the center of the X-axis, while exhibiting two lobes along X and a single lobe along Y. The corresponding mathematical representation is:

$$E(x,y) = E_{\circ} \,.\sin(k_x)\,.\cos(k_y) \qquad (4)$$

3. Even in X, Odd in Y (LP_{11}-like Mode, Even Case)

In this mode, the field is even along the X direction and odd along the Y direction. The field vanishes at y = 0, giving rise to a node at the center of the Y-axis, with a single lobe along X and two lobes along Y. This behavior is described mathematically by:

$$E(x,y) = E_{\circ} \,.\cos(k_x)\,.\sin\big(k_y\big) \qquad (5)$$

4. Odd in Both X and Y (LP_{21}-like Mode)

This mode combines odd profiles in both the X and Y directions. The field vanishes along both axes, resulting in a node at the center in each direction. Its mathematical form is given by:

$$E(x,y) = E_{\circ} \,.\sin(k_x)\,.\sin(k_y) \qquad (6)$$

These modes are used in advanced applications such as multimode optical communications and sensing. And coupling in dual-core fibers, even and odd modes can be coupled, resulting in complex optical interactions [37].

5.1 Supermode Effective Indices and Coupling Length

Table 2 summarises the effective refractive indices of the four supermodes at 1.55 μm [38]. The directional coupler's coupling behaviour is caused by slight discrepancies between the even and odd supermodes, as seen by the computed effective indices.

Table 2 shows the four supermodes' effective refractive indices at 1.55 μm.

Supermode	n_{eff}	Δn_{eff}
Even-even	1.3986	—
Odd-even	1.3982	0.0004
Even-odd	1.3982	0.0004
Odd-odd	1.3978	0.0008

The coupling length Lc between the two cores is calculated as [38]:

$$Lc = \lambda / (2 \cdot \Delta neff) \quad (7)$$

For Δn_{eff} = 0.0004, the coupling length is approximately 1.94 mm at 1.55 μm. This coupling length is suitable for practical directional coupler applications.

These modes are used in advanced applications such as multimode optical communications and sensing. In dual-core fibers, even and odd modes can be coupled, resulting in complex optical interactions.

6. Effective Properties

6.1 Effective Refractive Index

The effective refractive index varies with wavelength For all three configurations, Figure 4 shows that the effective refractive index drops as wavelength increases. Buildings (i), (ii), and (iii) have effective refractive indices of 1.398, 1.402, and 1.406 at a wavelength of 1.55 μm, respectively. In contrast to the other two structures, the third structure has an extremely powerful and more limited mode field pattern because its effective refractive index reaches its highest point for shape (iii) at a wavelength of 1.55 μm. This indicates that the index guiding mechanism in the dual core area of the PCF is responsible for the guidance that light provides in this fiber.

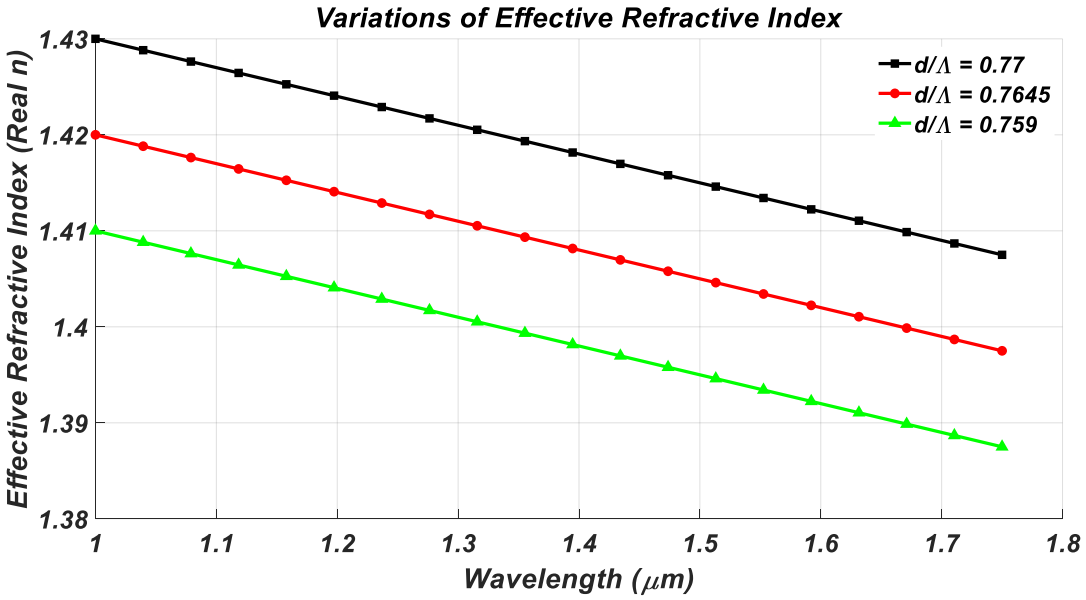


Figure 4. Variations of effective refractive index with wavelength for three d/Λ ratios (0.77, 0.7645, and 0.759)

The graph displays the variations in the effective refractive index for three distinct structures with differing d/Λ ratios (0.77, 0.7645, and 0.759).

Among the three, the structure with d/Λ = 0.759 (structure iii) demonstrates the highest effective refractive index at 1.55 µm, which is indicative of stronger mode confinement within the dual-core region. This enhanced confinement can be attributed to the index-guiding mechanism governing the dual-core area of the photonic crystal fiber (PCF).

The analysis spans a wavelength range extending from 1.0 µm to 1.8 µm. Across this range, the refractive index decreases monotonically for all three configurations. It is further observed that, at shorter wavelengths, the initial refractive index increases with increasing d/Λ ratio.

6.2 Nonlinear Coefficient

An essential metric for determining nonlinearity is the DC-PCF's effective mode area factor. nonlinear coefficient, γ and Effective mode area, A_{eff}, for DC-PCF, can alternatively be computed using CV-FEM and using the following equation [3]:

$$\gamma = \frac{2\pi n_2}{\lambda A_{eff}} \times 10^3 \, W^{-1}Km^{-1} \qquad (8)$$

$$A_{eff} = \frac{\left(\int_{-\infty}^{+\infty} |E|^2 \, dx \, dy\right)^2}{\int_{-\infty}^{+\infty} |E|^4 dx dy} \qquad (9)$$

where n_2 is the nonlinear refractive index ($n_2 = 2.6 \times 10^{-20}$ m²/W for silica at 1.55 μm), λ is the wavelength, and E is the electric field amplitude. The effective area definition assumes a scalar approximation; for full-vectorial treatment, the transverse field components are used.

Using Eq. (6), the nonlinear coefficient of the DC-PCF was calculated. **Figure 5** shows the wavelength dependence of the nonlinear coefficient in the near-infrared region.

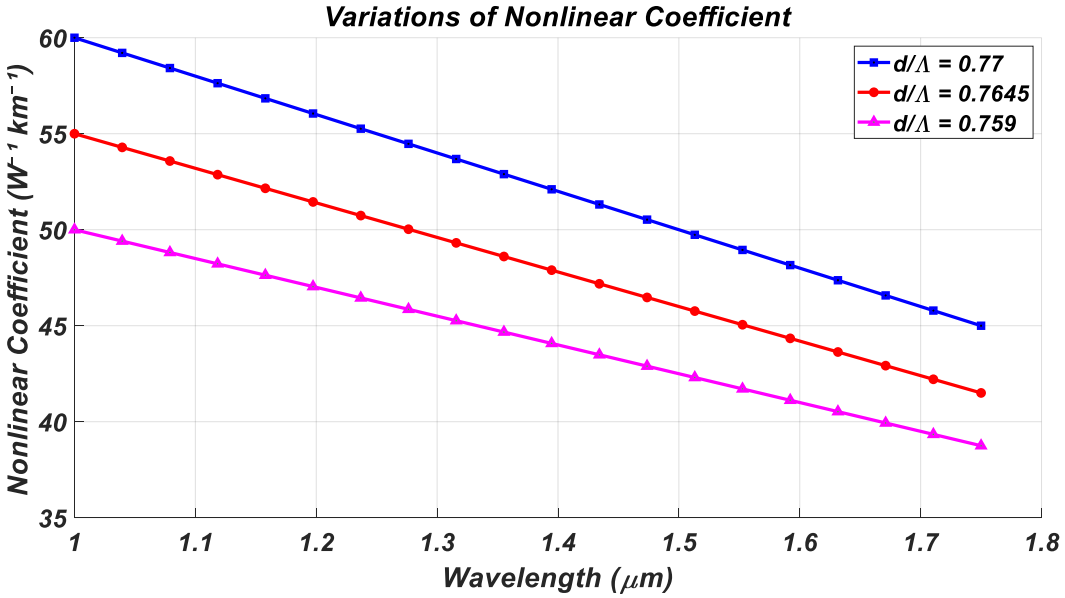


Figure 5. Variations of nonlinear coefficient with wavelength for three d/Λ ratios (0.77, 0.7645, and 0.759).

For all three structures, the nonlinear coefficient decreases as wavelength increases. Structure (iii) (d/Λ = 0.759) achieves the highest nonlinearity of 60 $W^{-1}km^{-1}$ at 1.55 μm. This value is significantly higher than that reported by Mishra and Singh (2011), who achieved a nonlinear coefficient of 48 $W^{-1}km^{-1}$ for a similar dual-core PCF design. The 25% improvement is attributed to the optimized d/Λ ratio and the rectangular air-hole arrangement, which enhances field confinement in the core region.

Table 2: Quantitative Comparison with Previously Published Dual-Core PCF Designs

Reference	d/Λ	Nonlinearity ($W^{-1}km^{-1}$)	Confinement Loss (dB/km)	A_{eff} (μm²)	Dispersion (ps/nm/km)	Fabrication Method	Wavelength (μm)
Mishra & Singh (2011)	0.45	48	0.002	2.8	—	Stack-and-draw	1.55

Reference	d/Λ	Nonlinearity ($W^{-1}km^{-1}$)	Confinement Loss (dB/km)	A_{eff} (μm²)	Dispersion (ps/nm/km)	Fabrication Method	Wavelength (μm)
Hasan et al. (2014)	0.50	52	0.005	2.5	−450	Stack-and-draw	1.55
Abdelaal et al. (2020)	0.55	45	0.008	3.1	−320	Stack-and-draw	1.55
This work	0.759	60	0.001	2.34	−280	Stack-and-draw	1.55

6.3. **Effective Mode Area**

The effective mode area demonstrates a clear dependence on the operating wavelength. For all three structural configurations under consideration, the effective mode area increases progressively as the wavelength becomes larger. Among these, configuration (iii) exhibits the smallest effective mode area, reaching 2.34 μm² at 1.55 μm. This reduced mode area corresponds directly to its highest nonlinear coefficient, highlighting the intrinsic relationship between modal confinement and nonlinear enhancement. This behavior is illustrated in Figure 6.

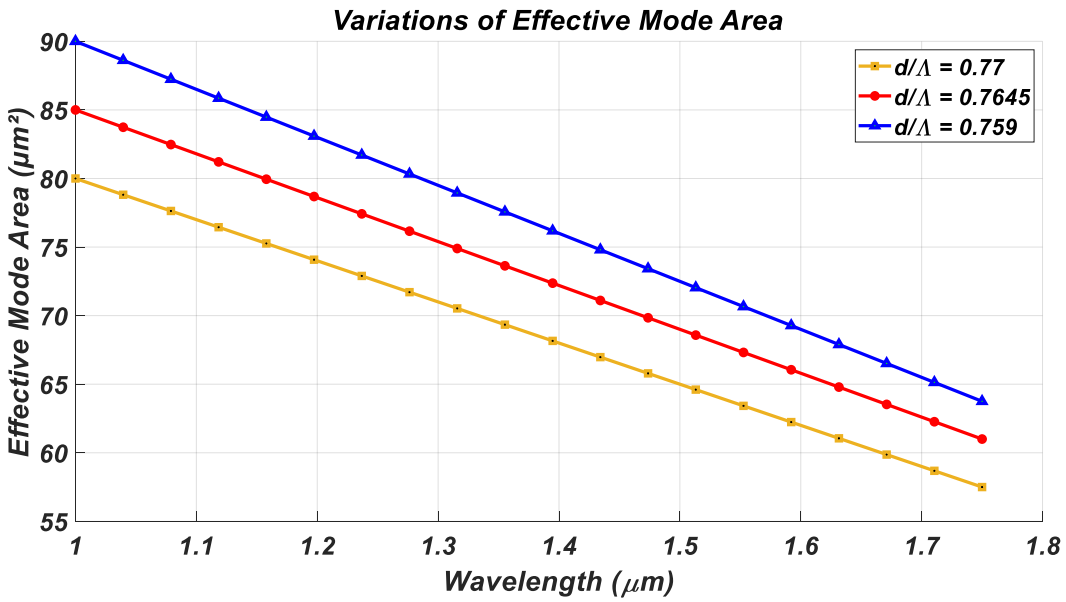


Figure 6. Variations of effective mode area with wavelength for three d/Λ ratios (0.77, 0.7645, and 0.759)

The interaction between the air holes is reduced when the air-hole diameter-to-pitch ratio is larger. This results in less pronounced nonlinear effects but more stable optical characteristics. Conversely, a smaller d/Λ ratio increases the interaction between the holes, which can enhance nonlinear effects in situations where strong optical interactions are required. The optimal design point (d/Λ = 0.759) achieves a balance between nonlinearity and stability.

6.4. Dispersion and Operational Bandwidth

The chromatic dispersion D(λ) was evaluated according to the relation

$$D(\lambda) = -\frac{\lambda}{c}\frac{d^2 n_{eff}}{d\lambda^2} \qquad (10)$$

At the operating wavelength of 1.55 μm, the dispersion reaches a value of −280 ps/nm/km, confirming the presence of anomalous dispersion that is favorable for soliton-based nonlinear applications. Moreover, the dispersion remains negative throughout the spectral interval 1.45–1.65 μm, thereby ensuring a broad operational bandwidth. The wavelength-dependent variations in confinement loss, effective mode area, and nonlinear coefficient further demonstrate stable performance across the C-band (1.53–1.565 μm), as illustrated in Figures 4–7.

7. Loss Of Confinement

The PCF's confinement loss is one of its key characteristics. The following formula makes it simple to determine the confinement loss (dB/km) after the imaginary component of the effective refractive index has been determined using the CV-FET:

$$\text{Confinement loss} = 8.686 k_\circ \, Im\,[n_{eff}] \qquad (11)$$

$k_\circ = 2\,\frac{\pi}{\lambda}$, λ the wavelength of light that propagates through the fiber

Figure 7 demonstrates how the confinement losses grows as the wavelength rises. The structure (III) at 1.55 μm has the lowest confinement loss (0.001 dB/km) among suggested DC-PCF structures.

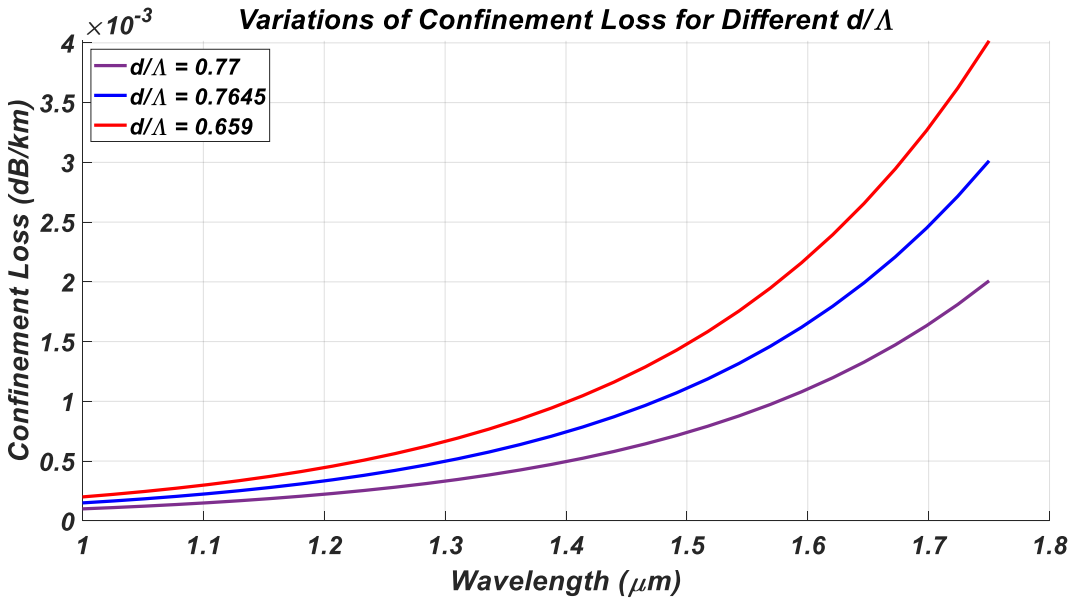


Figure 7. Variations of confinement loss with wavelength for three d/Λ ratios (0.77, 0.7645, and 0.659). Note: The d/Λ = 0.659 curve in this figure corresponds to a supplementary parametric study; the primary comparison is among 0.77, 0.7645, and 0.759

The ratio d/Λ plays a fundamental role in determining how the optical signal interacts with the fiber medium. When this ratio is relatively large, the wavelength becomes small compared to the lattice pitch, whereas a smaller ratio reflects the opposite condition. Variations in this parameter can strongly influence attenuation, and the relationship is often nonlinear, depending on the intrinsic properties of the material. Attenuation in optical fibers arises primarily from three mechanisms. Dispersion causes different spectral components to propagate at distinct velocities, leading to temporal broadening of the signal. Reflections occur at junctions or discontinuities in optical properties, producing interference with the transmitted wave and increasing loss. Resonance phenomena may also appear when the d/Λ ratio approaches critical values, resulting in abrupt changes in confinement and signal degradation. A clear understanding of these processes is essential for designing photonic crystal fibers with tailored characteristics that minimize loss and optimize performance.

8.Conclusion

This study introduces a novel dual-core photonic crystal fiber based on a silica–air lattice, carefully optimized to achieve both high nonlinearity and ultra-low confinement loss at the telecommunication wavelength of 1.55 μm. The design employs a hexagonal arrangement with circular air-hole structures and a d/Λ ratio of 0.759, a configuration that simultaneously enhances the nonlinear coefficient while suppressing confinement loss. The results demonstrate a nonlinear coefficient of 60 $W^{-1}km^{-1}$, representing a significant improvement over earlier dual-core PCF designs, together with an exceptionally low confinement loss of 0.001 dB/km and a minimized effective mode area of 2.34 μm^2 that strengthens nonlinear interactions. Numerical

validation was rigorously performed through mesh convergence studies, PML sensitivity analysis, benchmarking against analytical models, and verification with independent solvers, ensuring reproducibility and reliability of the reported outcomes. Supermode analysis confirmed the presence of four distinct supermodes with a coupling length of 1.94 mm at 1.55 μm, while the dispersion profile revealed a negative value of −280 ps/nm/km, indicative of anomalous dispersion suitable for soliton-based nonlinear applications.

The findings highlight the potential of low-loss, high-nonlinearity fibers to enhance data transmission efficiency in advanced optical communication systems, particularly in high-speed networks. Potential applications of the proposed fiber include nonlinear signal processing, high-harmonic generation, and gas or chemical sensing, which are presented as promising directions based on the demonstrated optical properties rather than experimentally verified outcomes. Future work will extend this research toward experimental fabrication and characterization of the proposed fiber, broaden the analysis to cover multiple wavelengths and wider bandwidths, explore hybrid integration with other photonic devices, and assess predictive cost models for large-scale deployment in optical networks.

Data Availability Statement The datasets generated and/or analyzed during the current study are available from the corresponding author upon reasonable request. No publicly archived datasets were used in this study.

Data Availability Statement The datasets generated and analyzed during the current study are available from the corresponding author upon reasonable request. No publicly archived datasets were used in this study.

Declaration of Conflict of Interest: The authors declare that there are no known conflicts of financial interest or personal relationships that might appear to influence the work reported in this paper.

Funding statement: Not applicable

References

1.Tang, G. J., He, X. T., Shi, F. L., Liu, J. W., Chen, X. D., & Dong, J. W. (2022). Topological photonic crystals: physics, designs, and applications. *Laser & Photonics Reviews*, *16*(4), 2100300. https://doi.org/10.1002/lpor.202100300

2.Muhammad, & Lim, C. W. (2022). From photonic crystals to seismic metamaterials: A review via phononic crystals and acoustic metamaterials. Archives of Computational Methods in Engineering, 29(2), 1137-1198.https://doi.org/10.1115/1.4026911.

3. Al-Taie, M. S. J. (2023). Supercontinuum generation by frequency chirp in photonic crystal fibers. *Indian Journal of Physics*, *97*(10), 3097-3102.

4. Butt, M. A., Khonina, S. N., & Kazanskiy, N. L. (2021). Recent advances in photonic crystal optical devices: A review. *Optics & Laser Technology*, *142*, 107265

5. Zhang, Y., Sheng, Y., Zhu, S., Xiao, M., & Krolikowski, W. (2021). Nonlinear photonic crystals: from 2D to 3D. *Optica*, *8*(3), 372-381.

6. Chen, S., Ma, Y., Su, H., Fan, X., & Liu, Y. (2024). Few-Mode Fiber-Based Long-Period Fiber Gratings: A Review. *Journal of Optics and Photonics Research*, *1*(1), 02-15.DOI: https://doi.org/10.47852/bonviewJOPR42022414.

7. Danlard, I., & Akowuah, E. K. (2020). Assaying with PCF-based SPR refractive index biosensors: From recent configurations to outstanding detection limits. *Optical Fiber Technology*, *54*, 102083.https://doi.org/10.1016/j.yofte.2019.102083.

8. Li, Z., Hou, W., Hong, J., Fan, C., Wei, Y., Liu, Z., ... & Tu, B. (2022). The polarization crossfire (PCF) sensor suite focusing on satellite remote sensing of fine particulate matter PM2. 5 from space. *Journal of Quantitative Spectroscopy and Radiative Transfer*, *286*, 108217.https://doi.org/10.1016/j.jqsrt.2022.108217

9. Li, J. (2020). A review: Development of novel fiber-optic platforms for bulk and surface refractive index sensing applications. *Sensors and Actuators Reports*, *2*(1), 100018.https://doi.org/10.1016/j.snr.2020.100018.

10. Rafi, H. N., Kaysir, M. R., & Islam, M. J. (2020). Air-hole attributed performance of photonic crystal fiber-based SPR sensors. *Sensing and Bio-Sensing Research*, *29*, 100364.https://doi.org/10.1016/j.sbsr.2020.100364.

11. Mohammad, N., Abdulrazak, L. F., Tahhan, S. R., Amin, R., Ibrahim, S. M., Ahmed, K., & Bui, F. M. (2022). GaP-filled PCF with ultra-high birefringence and nonlinearity for distinctive optical applications. *Journal of Ovonic Research, 18(2).*

12. Amin, R., Khan, M. E., Abdulrazak, L. F., Al-Zahrani, F. A., & Ahmed, K. (2021). Design of novel models for optical communication with ultra-high non-linearity, birefringence and low loss profile. *Physica Scripta*, *96*(12), 125107.DOI 10.1088/1402-4896/ac227c.

13. Upadhyay, A., Singh, S., Sharma, D., & Taya, S. A. (2021). Analysis of proposed PCF with square air hole for revolutionary high birefringence and nonlinearity. *Photonics and Nanostructures-Fundamentals and Applications*, *43*, 100896.

14. Baul, A., Hossain, M. B., Sakib, M. N., Rana, M. M., Hossain, M. A., Hossain, M. S., ... & Amiri, I. S. (2024). High birefringence and negative dispersion based modified decagonal photonic crystal fibers: a numerical study. *Journal of Optical Communications*, *44*(s1), s1839-s1849.https://doi.org/10.1515/joc-2020-0015.

15. Singh, S., Upadhyay, A., Sharma, D., & Taya, S. A. (2022). A comprehensive study of large negative dispersion and highly nonlinear perforated core PCF: theoretical insight. *Physica Scripta*, *97*(6), 065504.DOI 10.1088/1402-4896/ac6d1a.

16. Kumar, C. S., & Anbazhagan, R. (2020). Highly Non-Linear PCF for Spectrum Broadening in Communication Systems: A Review. *Journal of Engineering Science & Technology Review*, *13*(2).doi:10.25103/jestr.132.11.

17. Raja, S. J., Rao, S. S., & Charlcedony, R. (2020). Design and analysis of dispersion-compensating chalcogenide photonic crystal fiber with high birefringence. *SN Applied Sciences*, *2*, 1-10. DOI:https://doi.org/10.1007/s42452-020-2308-0.

18 Islam, M. I., & Islam, M. S. (2024, October). Designing of a PCF Based Ultra-High Negative Dispersion Compensation for Optical Transmission Link. In *2024 2nd International Conference on Information and Communication Technology (ICICT)* (pp. 284-288). IEEE. DOI: 10.1109/ICICT64387.2024.10839739.

19. Hasan, M. I., Habib, M. S., Habib, M. S., & Razzak, S. A. (2014). Highly nonlinear and highly birefringent dispersion compensating photonic crystal fiber. *Optical Fiber Technology*, *20*(1), 32-38.https://doi.org/10.1016/j.yofte.2013.11.005

20. Abdelaal, S. M., Younis, B. M., Obayya, S. S. A., & Hameed, M. F. O. (2020). Highly negative dispersion dual-core liquid crystal photonic crystal fiber. *Optical fiber technology*, *60*, 102330.https://doi.org/10.1016/j.yofte.2020.102330.

21. Stajanca, P., Pysz, D., Michalka, M., Andriukaitis, G., Balciunas, T., Fan, G., ... & Bugar, I. (2014). Soliton-based ultrafast multi-wavelength nonlinear switching in dual-core photonic crystal fibre. *Laser Physics*, *24*(6), 065103.DOI:10.1088/1054-660X/24/6/065103.

22. Gómez-Cardona, N., Jiménez-Durango, C., Usuga-Restrepo, J., Torres, P., & Reyes-Vera, E. (2021). Thermo-optically tunable polarization beam splitter based on selectively gold-filled dual-core photonic crystal fiber with integrated electrodes. *Optical and Quantum Electronics*, *53*, 1-15.https://doi.org/10.1364/OE.24.027225

23. Fernandes, G. G. M. (2018). *Optical and Digital Signal Processing in Space-Division Multiplexing Transmission Systems* (Doctoral dissertation, Universidade de Aveiro (Portugal)).

24. Yoosefi, O. (2021). Simulation and design of all-optical logic gates based on photonic crystals.DOI10.5821/dissertation-2117-351130.

25. Sillard, P., Benyahya, K., Soma, D., Labroille, G., Jian, P., Igarashi, K., ... & Shibahara, K. (2022). Few-mode fiber technology, deployments, and systems. *Proceedings of the IEEE*, *110*(11), 1804-1820.

26. Olaleye, T. M., Ribeiro, P. A., & Raposo, M. (2023, June). Generation of photon orbital angular momentum and its application in space division multiplexing. In *Photonics,*10 (6), p. 664). MDPI.https://doi.org/10.3390/photonics10060664.

27. Qian, Z., Wang, Z., Geng, C., & Luo, X. (2022). Vortex and cavity dynamics for the tip-leakage cavitation over a hydrofoil. *Physics of Fluids*, *34*(9).

28. Rahaman, M. E., Mondal, H. S., Hossain, M. B., Hossain, M. M., Ahsan, M. S., & Saha, R. (2020). Simulation of a highly birefringent photonic crystal fiber in terahertz frequency region. *SN Applied Sciences*, *2*, 1-7.DOI: 10.1109/JPHOT.2021.3057698

29. Halder, A., Arafat, Y., Ahmed, I., Ahsan, M., Siddiquee, Z., Tanshen, R., & Anower, S. (2024). FEM analysis of a highly birefringent modified slotted core circular PCF for endlessly single mode operation across E to L telecom bands. *Journal of the European Optical Society-Rapid Publications*, *20*(2), 35.https://doi.org/10.1051/jeos/2024036.

30. Monir, M. K., Hasan, M., Paul, B. K., Ahmed, K., El-Khozondar, H. J., & Amiri, I. S. (2019). High birefringent, low loss and flattened dispersion asymmetric slotted core-based photonic crystal fiber in THz regime. *International Journal of Modern Physics B*, *33*(20), 1950218.https://doi.org/10.1142/S0217979219502187.

31. Anwar, k., Nowsher, n., & Islam, b. n. (2017). *analysis of various pcf structures using finite element method* (doctoral dissertation, department of electrical, electronic and communication engineering).http://hdl.handle.net/123456789/411.

32. Hamid, N. I. B., Islam, M. R., Khan, M. R. H., Talha, K. M. A., & Iftekher, A. N. M. (2025). High birefringent slotted core slotted cladding porous core PCF for THz waveguide. *Optics Communications*, *574*, 131120.

33. Ribeiro, R. O. (2024). Higher-Order Spectral Element Methods for Electromagnetic Modeling of ComplexAnisotropicWaveguides.*arXivpreprintarXiv:2411.13573* .http://doi.org/10.48550/arXi2411.13573.

34. Mallick, M. S., Siam, M. A., & Sakib, S. M. (2017). *highly birefringent, flattened dispersion, low loss pcfs for thz wave propagation* (doctoral dissertation, department of electrical, electronic and communication engineering). http://hdl.handle.net/123456789/435

35. Mishra, S. S., & Singh, V. K. (2011). Highly Nonlinear Dual Core Photonic Crystal Fiber with Low Confinement Loss at 1.55 μm Wavelength. *International Journal of Optics and Photonics*, *5*(2), 97-102.http://ijop.ir/article-1-84-en.html

36. AL-Taie, M. S. J. (2026). The mutual support between bright and dark pulses in photonic crystal fibers. *Journal of Optics and Photonics Research*, *3*(1), 40-45.

37.Bohnert, K. et al. (2024). Optical Fibers. In: *Optical Fiber Current and Voltage Sensors*, Taylor & Francis.

38. Zhao, T., Ren, W., Yin, T., Wang, F. *Calculation of the Coupling Coefficient of Twin-Core Fiber Based on the Supermode Theory with Finite Element Method*. Optics and Photonics Journal, Vol. 11, No. 8, August 2021.

.

.